

Microstructure evolution of threeroll skewrolling formed hollow axles with uniform wall thickness

Shu, Chang; Zhang, Song; Bidare, Prveen; Essa, Khamis; Abdelwahab, Adel; Shu, Xuedao; Pater, Zbigniew; Bartnicki, Jaroslaw

DOI:

[10.1007/s00170-022-09583-5](https://doi.org/10.1007/s00170-022-09583-5)

License:

Creative Commons: Attribution (CC BY)

Document Version

Publisher's PDF, also known as Version of record

Citation for published version (Harvard):

Shu, C, Zhang, S, Bidare, P, Essa, K, Abdelwahab, A, Shu, X, Pater, Z & Bartnicki, J 2022, 'Microstructure evolution of threeroll skewrolling formed hollow axles with uniform wall thickness', *The International Journal of Advanced Manufacturing Technology*, vol. 121, no. 5-6, pp. 4069-4085. <https://doi.org/10.1007/s00170-022-09583-5>

[Link to publication on Research at Birmingham portal](#)

General rights

Unless a licence is specified above, all rights (including copyright and moral rights) in this document are retained by the authors and/or the copyright holders. The express permission of the copyright holder must be obtained for any use of this material other than for purposes permitted by law.

- Users may freely distribute the URL that is used to identify this publication.
- Users may download and/or print one copy of the publication from the University of Birmingham research portal for the purpose of private study or non-commercial research.
- User may use extracts from the document in line with the concept of 'fair dealing' under the Copyright, Designs and Patents Act 1988 (?)
- Users may not further distribute the material nor use it for the purposes of commercial gain.

Where a licence is displayed above, please note the terms and conditions of the licence govern your use of this document.

When citing, please reference the published version.

Take down policy

While the University of Birmingham exercises care and attention in making items available there are rare occasions when an item has been uploaded in error or has been deemed to be commercially or otherwise sensitive.

If you believe that this is the case for this document, please contact UBIRA@lists.bham.ac.uk providing details and we will remove access to the work immediately and investigate.



Microstructure evolution of three-roll skew-rolling formed hollow axles with uniform wall thickness

Chang Shu¹ · Song Zhang² · Prveen Bidare¹ · Khamis Essa¹ · Adel Abdel-Wahab⁴ · Xuedao Shu² · Zbigniew Pater³ · Jaroslaw Bartnicki³

Received: 6 April 2022 / Accepted: 16 June 2022
© The Author(s) 2022

Abstract

The uniform thickness hollow axle is one of the lightest weight axles in the high-speed rail industry. It can effectively reduce unsprung mass and further improve the train speed. Therefore, due to its importance and significance, it is crucial to research and develop the uniform thickness hollow axle. To understand the microstructural evolution during three-roll skew-rolling (TRSR) forming, 30CrMoA alloy steel was used in this study. A constitutive model of 30CrMoA was established by SIMU-FACT FORMING finite element software and utilized to simulate the deformation, heat transfer, and microstructure coupling during TRSR. Via analyzing the influence of process parameters on the average grain size, the microstructural evolution of the forming part at each deformation stage is revealed. The result shows that the dynamic recrystallization of the rolled piece produces a fine and uniform grain structure during the forming process. The refinement level is enhanced with the increase of the radial compression; the grain size is gradually increased from the outer surface to the inner surface of the rolled piece. At a higher rolling temperature, it was found the initial grain size and final average grain size were larger compared to the lower temperature. By increasing the axial traction speed, not only can the rolling time be shortened, but also the appearance of coarse grains can be avoided. Therefore, the mechanical properties can be improved.

Keywords Three-roll skew-rolling forming · 30CrMoA · Hollow axle · Microstructure evolution · Finite element analysis

1 Introduction

With the rapid growth of the global economy during the past decades, high-speed rail (HSR) plays an important role in modern society. Both the USA and China have put the agenda on developing the next generation of high-speed rail in their next 10 years plan [1, 2]. The HSR speed is a critical assessment of the performance of the rail. Thus, how to improve the HSR speed is a significant topic for engineers and researchers. One of the solutions to further improve the

train speed is achieving the lightweight structure of the rail vehicle.

The hollow axle is a new genre of axle design; it not only meets the requirement of strength but also greatly reduces the unsprung weight of the rail, meanwhile maintaining stability and safety; therefore, it is one of the most effective ways to realize the lightweight. Based on the different structural designs of the internal hole, the hollow axle is divided into two categories: the hollow axle with an equal diameter and the hollow axle with a uniform wall thickness. For the hollow axle with equal diameter, as its internal diameter is fixed, the manufacturing process is mainly multi-process forging and deep hole drilling [3, 4], as well as the integrated forming of cross wedge rolling with mandrel [5, 6]. For the hollow axle with uniform wall thickness, the wall thickness is the same all along the axle. However, a uniform thickness axle is more difficult to manufacture than an equal diameter axle due to its geometrical complexity; on the other hand, due to its prominent mechanical properties and even better lightweight performance [7, 8], studying its net near forming method and microstructure evolution will promote the

✉ Chang Shu
cxs176@student.bham.ac.uk

¹ Department of Mechanical Engineering, University of Birmingham, Birmingham B15 2TT, UK

² Faculty of Mechanical Engineering and Mechanics, Ningbo University, Ningbo, China

³ Faculty of Mechanical Engineering, Lublin University of Technology, Lublin, Poland

⁴ Department of Mechanical Engineering, University of Birmingham Dubai, Dubai, UAE

development of high-speed rail and eventually achieve the higher speed of rail vehicle.

Fabrication of the uniform thickness hollow axle is challenging due to the nature of its multiple internal diameters along the axle. Typically, the internal hole is processed by precision forging and deep drilling. This procedure usually cuts off the metal fiber, which could be detrimental to the mechanical performance [9]. In this study, a novel forming method has been applied, which is the three-roll skew-rolling (TRSR) process [10]. This method is a die-free flexible forming technique that can form different shapes of axles by real-time controlling the distance between the rolls, and compared to traditional machining, forging, or cross wedge rolling process; it has the following advantages: higher utilization rate, higher efficiency, lower cost, and less environmental pollution. Thus, it plays an important role in advanced near-net-shape manufacturing technology [11, 12]. Several studies have been carried out on the three-roll skew rolling process. Zhang et al. [13] and Cao et al. [14] analyzed the forming of titanium alloy rods with equal diameter in the TRSR process and obtained the relation between the processing parameters and forming quality. Xu and Shu [15] used SIMUFACT finite element software to simulate the TRSR forming process. The simulated model was scaled down to 1:5 compared to the high-speed train hollow axle, and the stress–strain field, temperature field, rolling force, and metal flow field were analyzed in detail. The results showed that force and energy parameters were significantly smaller than those in cross wedge rolling, further verifying the feasibility of this process. Stefanik et al. [16] provided theoretical and experimental support for forming aluminum rods by the TRSR process. Gryc et al. [17] studied the influence of process parameters on temperature field in rolled part during TRSR. Markov et al. [18]. studied the forging process of pipe without a mandrel, and the results show that the main factor affecting wall thickening is the inner diameter; it was found that a relative inner diameter between 0.55 and 0.60 recommended for the maximum thickening of a forging wall. Pater et al. [19–22] used the finite element simulation and experimental validation to study the Ti6AL4V hollow shaft in trucks and cars, and provided theoretical foundations on long-shaft parts by TRSR. Bartnicki et al. [23] designed and built their own TRSR mill machine to form the hollow axle. The feature of this mill enables the precision movement of rolls and clamps by programming in the CNC system. Therefore, a more geometrically complex and accurate part can be obtained. Zhang et al. [4, 7, 24, 25] simulated the process of hollow axles during TRSR and studied the effect of processing parameters on the uniformity of wall thickness. They analyzed the formation mechanism of spiral-like defects on the part surface.

The above research mainly emphasizes mechanical properties and geometrical accuracy control. There are very

few studies that focus on micro-scale investigations such as microstructure evolution and defects generated during the forming process. To achieve comprehensive and accurate TRSR, it is necessary not only to meet the geometrical requirements of the rolled part, but also to understand the formation of the microstructure to further improve the mechanical performance. Due to the material deformation and high-temperature environment in the hot forming process as TRSR, the microstructure of the material will undergo a series of changes such as static-dynamic recrystallization and grain growth. These changes will determine the mechanical performance of the final rolled piece. Therefore, this study aims the microstructure evolution of hollow axles during the TRSR process by evaluating simulated results and experimental results. These phenomena were investigated on 30CrMoA structural steel by analyzing its grain size evolution under multiple processing conditions and exploring the formation mechanism behind the grain distribution.

2 Model and experiment

2.1 Kinematic model

The main characteristic of three-roll skew rolling is that the rolled part moves forward spirally. With the rolling continuing, the rolled part eventually reaches the desired geometry. The principle of generating this spiral movement has mainly two reasons: (1) The three rolls all rotate in the same direction. (2) The rolling line is inclined to roller axis by a feed angle β . Figure 1 shows the schematic of the TRSR process and the velocity vectors in different cross-section planes.

The linear velocity at any point P in the deformation zone is v_p ; by projecting the velocity vector v_p , the axial components (v_{px}) and tangential components (v_{py}) can be obtained and are shown in Eqs. (1) and (2). The lead distance Z_x that the rolling part moves along the rolling direction per revolution, is shown in Eq. (3). The pitch distance z_x that the rolling part moves along the rolling direction every processing time, is shown in Eq. (4). η_x and η_y are the axial and tangential slip coefficients of point P in the deformation zone, respectively.

$$v_{px} = v_p \cos \varphi \sin \beta \quad (1)$$

$$v_{py} = v_p \cos \varphi \cos \beta \cos \gamma - v_p \sin \varphi \sin \gamma \quad (2)$$

$$Z_x = \frac{60}{n_b} u_{px} = 2\pi r_p \frac{\eta_x}{\eta_y} \frac{\cos \varphi \sin \beta}{\cos \varphi \cos \beta \cos \gamma - \sin \varphi \sin \gamma} \quad (3)$$

$$z_x = Z_x/3 = \frac{2\pi r_p}{3} \frac{\eta_x}{\eta_y} \frac{\cos \varphi \sin \beta}{\cos \varphi \cos \beta \cos \gamma - \sin \varphi \sin \gamma} \quad (4)$$

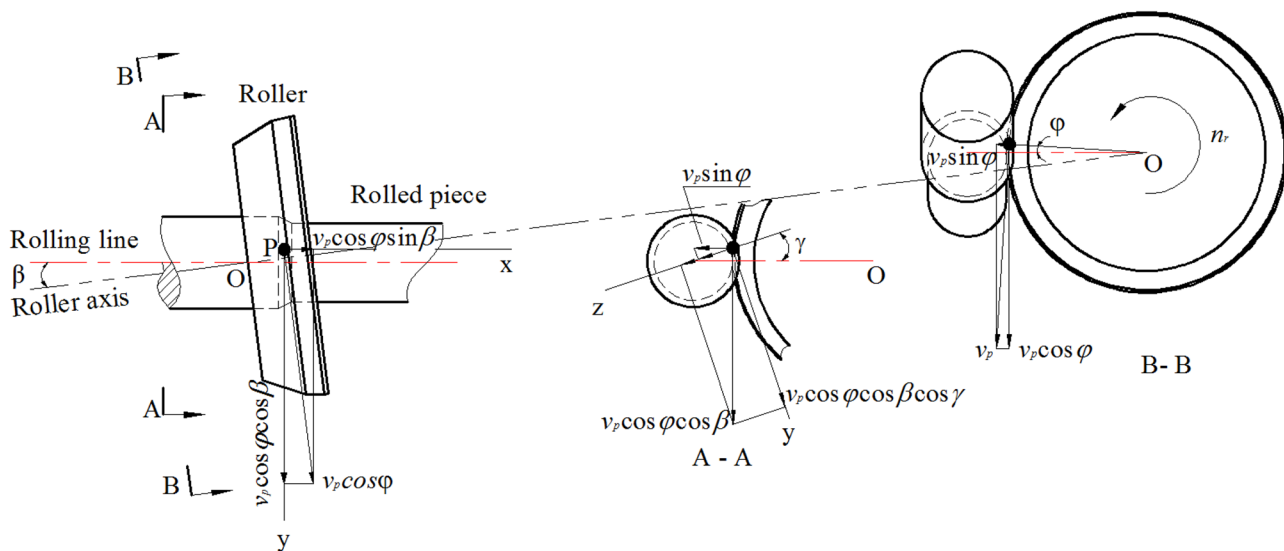


Fig. 1 Velocity vector of any point in the deformation zone of the three-roll skew-rolling process

It is important to minimize or diminish the spiral-like defect on the surface of the rolled part. To achieve the spiral-free process, one of the solutions is to control the pitch distance either equal to or smaller than a certain value when forming in the region of multiple diameters [4, 25]. According to Eqs. (3) and (4), adjusting either the axial traction speed or rotational speed of the rolls can control the pitch to the optimal results. In the diameter increasing region, gradually lower the axial traction speed or increase rotational speed, or in the diameter decreasing region, increase the axial traction speed or lower rotational speed.

2.2 Material model

The material used in this study is 30CrMoA steel, which is a medium carbon structural steel with excellent hardenability, strength, and toughness. It has many advantages over other conventional steels, and it was designed to be applied on 300~350 km/h high-speed rail fields. Previous studies [26, 27] reported that 30NiCrMoV12 steel had outstanding mechanical properties and fatigue properties. In particular, the tensile test of the rail axle can reach 1000 MPa and the notched fatigue test reached 356 MPa; it was even better in the impact test at low temperature. In the full-scale physical fatigue tests, the axle successfully passed the tests, and under the condition of a speed of 350 km/h, the safety factor was around 1.99, which significantly improved the safety level. Due to the similar chemical composition with 30NiCrMoV12, 30CrMoA has been developed to replace the 30NiCrMoV12 because of the cheaper manufacturing cost

and the promising properties that has been shown in the previous study [28]. The chemical composition of 30CrMoA steel is shown in Table 1. The material properties of the billet were obtained from experiments and are presented in Table 2.

Constitutive relations of 30CrMoA steel are obtained and imported into the material bank of finite element software. The material models are described in the previous studies [28, 29], and are shown in Eqs. (5) and (6). Figure 2 was obtained from the compressive test, showing stress–strain relation of 30CrMoA under multiple conditions.

$$\sigma_p = 3756.3 \cdot e^{-0.003817 \cdot \epsilon} \cdot \epsilon^{0.08449} \cdot e^{-0.00306/\epsilon} \cdot \dot{\epsilon}^{0.16866} \quad (5)$$

$$\begin{cases} d_{dyn} = d_0 & (\bar{\epsilon} < \epsilon_c) \\ d_{dyn} = 4774.98 \times \dot{\epsilon}^{-0.0567} \times \exp[-60713/(RT)] & (\bar{\epsilon} \geq \epsilon_c) \\ \epsilon_c = 0.00767 \times \exp(3634.2/T) \end{cases} \quad (6)$$

where σ_p is the flow stress, MPa; ϵ is the equivalent strain; $\dot{\epsilon}$ is the strain rate, s^{-1} ; T is the temperature, $^{\circ}C$; d_{dyn} is the grain size of dynamic recrystallization, μm ; d_0 is the initial grain size, μm ; R is the gas constant ($8.314 J \cdot mol^{-1} \cdot K^{-1}$); $\bar{\epsilon}$ is the average strain; ϵ_c is the critical strain.

2.3 Finite element model

The three-dimensional model of three-roll skew rolling and hollow axle was built in the SOLIDWORKS software and

Table 1 Chemical composition of 30CrMoA alloy structural steel (wt%)

| C | Si | Mn | S | P | Cr | Ni | Cu | Mo |
|-----------|-----------|---------|--------------|--------------|-----------|--------------|--------------|-----------|
| 0.26~0.33 | 0.17~0.37 | 0.4~0.7 | ≤ 0.025 | ≤ 0.025 | 0.80~1.10 | ≤ 0.030 | ≤ 0.025 | 0.15~0.25 |

Table 2 Material properties of the billet

| Poisson ratio | Coefficient of thermal expansion (1/°C) | Emissivity(N/s/mm ² ·C ⁴) | Convection coefficient(N/s/mm ² ·C) | Density (kg/m ³) |
|---------------|---|--|--|------------------------------|
| 0.279 | 9.37209e ⁻⁶ | 0.8 | 0.02 | 7850 |

the STL format file was imported into SIMUFACT FORMING V14.0 software for the finite element analysis. The imported finite element model is shown in Fig. 3. Since the hollow axle belongs to a large-size long axle in real production, it will be very time-consuming to carry out the simulation with a 1:1 scale. Thus, to achieve the cost-effective simulation, a scale with a validated 1:5 model of the high-speed hollow axle is used to perform the finite element simulation in this study [22]. The CAD models of hollow axle and billet are shown in Fig. 4. The initial billet is the thick-walled hollow rod with 52-mm external diameter, 30-mm internal diameter, 11-mm thickness, and 500-mm length as shown in Fig. 4b. The chuck fixture and rolls are set as a rigid body. The hollow billet adopts 8-node hexahedral mesh elements with 31,752 mesh elements in total, and the entire duration of the rolling process is 27 s with 0.176 s per step. Noted that when equivalent strain is increased to 0.4, the adaptive model will automatically re-mesh to prevent the mesh distortion. Two different coefficients for shear friction are set, between roll and workpiece is 0.8, between fixture and workpiece is 1.0 [22]. The heat transfer coefficient in billet is set to be 15,000 W/(m²·K), and the heat transfer coefficient in the environment is 50 W/(m²·K). Two operating temperatures (1000 °C and 1100 °C), three different axial traction speeds (10 mm/s, 20 mm/s, and 30 mm/s), and three corresponding roll radial loading speeds were chosen

to study the processing parameter effect on the grain size. The detailed process parameters of finite element simulation are given in Table 3.

2.4 Experiment

The processing parameters and forming procedures are presented in Table 4 and Fig. 5, respectively. The rolled pieces are shown in Fig. 6. Microstructure sample is obtained by the following steps: (1) wire cutting along the axial direction; (2) take the samples from multiple chosen locations; (3) etching the sample by the saturated aqueous solution of picric. SU 5000 Field-Emission Scanning Electron Microscope (Hitachi, Japan) is used to observe the microstructure in samples. A total 11 different cross-sections are selected to obtain the microstructure sample as shown in Fig. 7. Outer, core, and inner layers are taken from each sample and are utilized to count the grain size. The intercept method is used to determine the average grain size by the NANO MEASURER 1.2 software. Noted No. 1 cross-section is the non-deformation area and it functions as the clamping fixture, and other cross-sections participate in the deformation as different forming diameters.

3 Results and discussion

3.1 Numerical simulation

3.1.1 Microstructure characteristics of hollow axle at different locations

The rolling conditions are set with a temperature $T=1100$ °C and an axial traction speed $V_z=20$ mm/s, to study

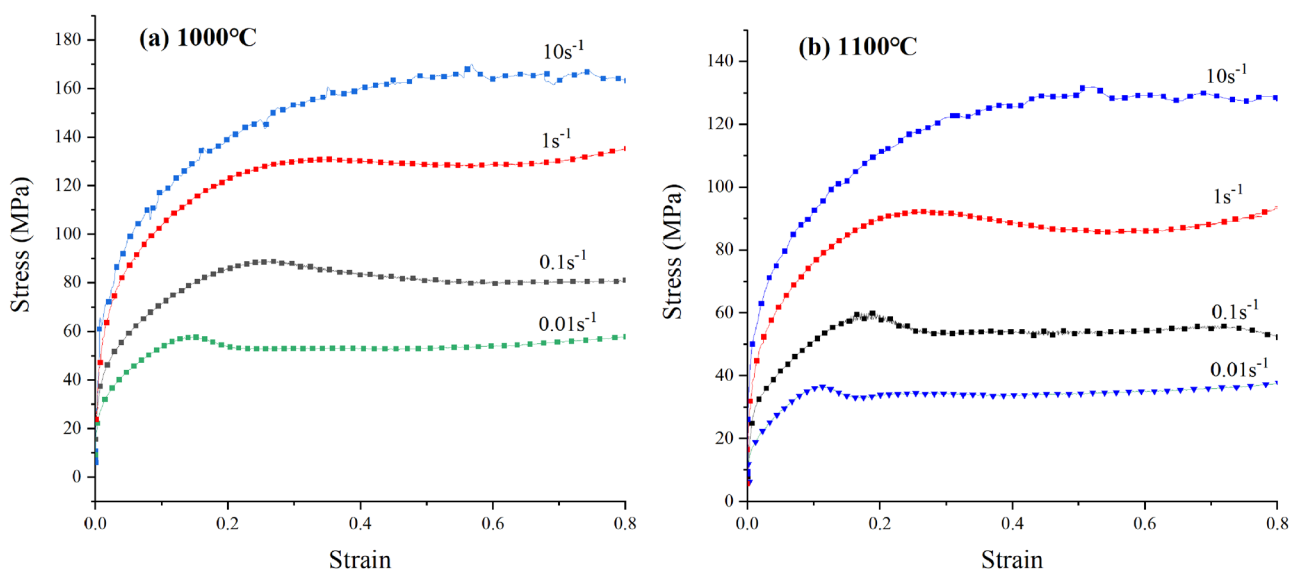
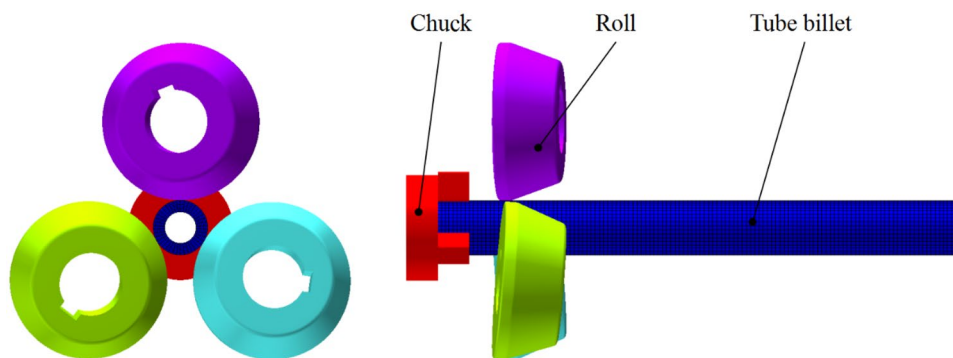
**Fig. 2** True stress–strain curve with different strain rates under two temperatures, **a** 1000 °C and **b** 1100 °C

Fig. 3 Finite element model of hollow axles formed by three-roll skew rolling

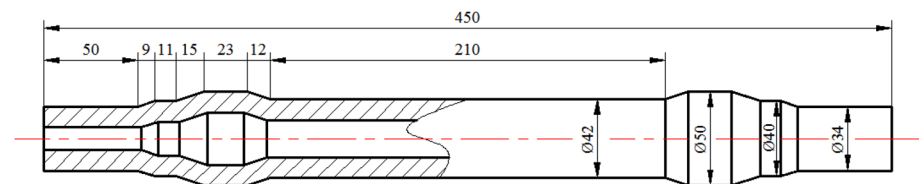


the characteristics of microstructure distribution in the 30CrMoA hollow axle. As shown in Fig. 8a, the grain refinement in the axle is quite significant compared to the initial grain size in the first deformed section due to the large radial compression and large contact area of the billet. As shown in Fig. 8b, the contact area between roll and workpiece is smaller in the second deformed section, and the grain size in the deformation zone is significantly smaller, whereas the grain size in the non-deformation zone is larger. The grain size in the third deformed section is larger than the grain size in the first and second deformed sections in Fig. 8c, indicating that greater radial compression results in smaller grain size. The diameter of the fourth deformed section is relatively larger in Fig. 8d, but the surface grain size is still significantly refined and uniformly distributed, indicating that the TRSR process can effectively improve surface microstructure quality. The fifth deformed zone is depicted in Fig. 8e with similar grain size and distribution results as in the third deformed section due to the identical radial compression. Figure 8f shows the sixth deformed section, the grain size is unevenly distributed along the rolling direction due to the influence of diameter reduction, and the grain size near the next deformation zone is smaller.

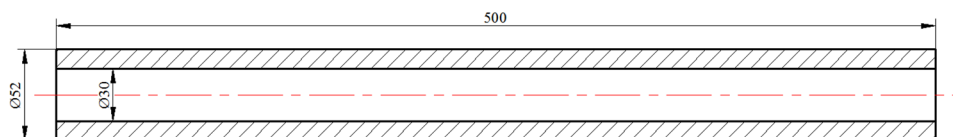
Figure 8g shows the seventh deformed section of the skew rolling, and it should be noted that the surface grain size is gradually decreasing along the rolling direction because the greater relative plastic deformation leads to more significant refinement. Overall, with the progress of rolling, the grain size of the already formed area will slightly increase. The average surface grain size is refined from 62.6 to 15–25 μm , demonstrating that the TRSR technique can refine the grain size and improve the microstructure properties of the hollow axle [10].

Figure 9 shows the distribution of grain size in the selected cross-sections at $T=1100\text{ }^\circ\text{C}$ and $V_z=20\text{ mm/s}$. The outer core and inner layer are defined in Fig. 9. It can be seen that the average grain size of the core and inner layer gradually increases along the rolling direction, while the change in the outer layer is negligible. The average grain size in the core is the largest and the average grain size in the direct contact area between roll and billet is the smallest. It can be observed that the grain is refined in the non-deformation zone but near the deformation area, and the grain size is reduced by half compared with the initial size. The average grain size in the deformed section is refined to 14.5–20 μm . The grain size in the core layer

Fig. 4 Dimensions of the hollow axle and axle billet. **a** 1:5 scale of high-speed train hollow axle. **b** CAD model of hollow billet



(a) 1:5 scale of high-speed train hollow axle.



(b) CAD model of hollow billet.

Table 3 Process parameter setting for finite element simulation of hollow axles in three-roll skew rolling

| Parameters | Unit | Values |
|---------------------------|------|------------------|
| Rolling temperature | °C | 1000, 1100 |
| Roll rotational speed | rpm | 60 |
| Axial traction speed | mm/s | 10, 20, 30 |
| Roll radial loading speed | mm/s | 0–3.5, 0–7, 0–10 |
| Roll tilt angle | ° | 5 |
| Roll forming angle | ° | 20 |
| Fine rolling width | mm | 12 |
| Diameter of roll | mm | 150 |

gradually increases along the rolling direction. Meanwhile, this pattern gradually diffuses to the inner layer, leading to similar grain size in the core and inner layer at the end of the workpiece.

The average grain size of the outer core and inner layer at different cross-sections is shown in Fig. 10 with $T = 1100\text{ °C}$ and $V_z = 20\text{ mm/s}$. From Fig. 10, the grain refinement in the outer layer is the most noticeable, especially at cross-sections F and G, while the core and inner have a similar trend of grain refinement. The grain size gradually increases along the rolling direction for both the core and inner layer, while the opposite pattern was found for the outer layer. Under the same amount of radial compression, the average grain size in core and inner layer is smaller at the early-stage rolling process, while the outer layer has the smaller grain size at the late stage of the rolling process. The results in Fig. 10 indicate that the rolling process has more influence on the grain refinement at the outer layer than at other layers, and the rolling sequence also plays an important factor in further refinement.

In summary, the three-roll skew-rolling process will promote the microstructure distribution and grain refinement, in particular at the outer surface layer; thus, the microstructure properties of the hollow axle can be improved via this process.

Table 4 The number of rolled piece and its processing parameter

| Roll piece | Rolling temperature (°C) | Axial traction speed (mm/s) |
|------------|--------------------------|-----------------------------|
| No. 1 | 1000 | 20 |
| No. 2 | 1100 | 20 |
| No. 3 | 1100 | 30 |
| No. 4 | 1100 | 10 |

3.2 Effect of processing parameters on average grain size

The rolling temperature has a significant effect on the grain size. Figure 11 compares the grain size of the inner and outer layer at 1000 °C and 1100 °C , to further understand the temperature effect. In Fig. 11, the initial grain size at 1100 °C is approximately three times greater than the grain size at 1000 °C , and the overall average grain size at 1100 °C is $5\text{ }\mu\text{m}$ greater than at 1000 °C . The curve pattern in the figure shows a similar trend of outer and inner layers between two temperatures, indicating the temperature mainly affects the grain size rather than changing other microstructure characteristics between outer and inner layers. Overall, the higher the rolling temperature, the larger the initial grain size, the larger the final grain size, but the relative changes in refinement are more significant at the higher temperature.

The axial traction speed directly affects the deformation rate and forming time, and potentially affects the temperature field during the process, resulting in the corresponding change in microstructure. Figure 12 shows the grain size distribution with different axial traction speeds at 1100 °C , 10 mm/s , 20 mm/s , and 30 mm/s . Figure 12a–c show the individual grain size distribution at each axial traction speed, and Fig. 12d shows the overall distribution with all three speeds included. Figure 12a indicates that radial compression has more influence on the grain size in outer layer than other layers. It can be seen from Fig. 12b, c the grain size distribution with 20 mm/s and 30 mm/s is similar, and only 30 mm/s has a slightly larger grain size than 20 mm/s . From Fig. 12d, the curve pattern for each speed is relatively unanimous, which indicates different axial traction speed has a similar effect on grain distribution in different layers. With increasing traction speed, the average grain size becomes larger in these layers. It should be noted that the increasing rate of grain size slows down when traction speed is adjusted from 20 to 30 mm/s . This is because, during the rolling process, the deformation zone will have more plastic deformation cycles, eventually resulting in more refined grains. When the axial traction speed is 20 mm/s , the curves have the smallest fluctuation rate, suggesting a more uniformly distributed microstructure along the axle.

It can be concluded that the rolling temperature has an imperative influence on the initial grain size. With the higher temperature, the grain size will be larger. However, the relative grain refinement is more significant. Furthermore, the greater the axial traction speed, the larger the grain size is. With the smaller traction speed, the relative grain refinement is more noticeable. It was found that 20 mm/s had a more evenly distributed microstructure.

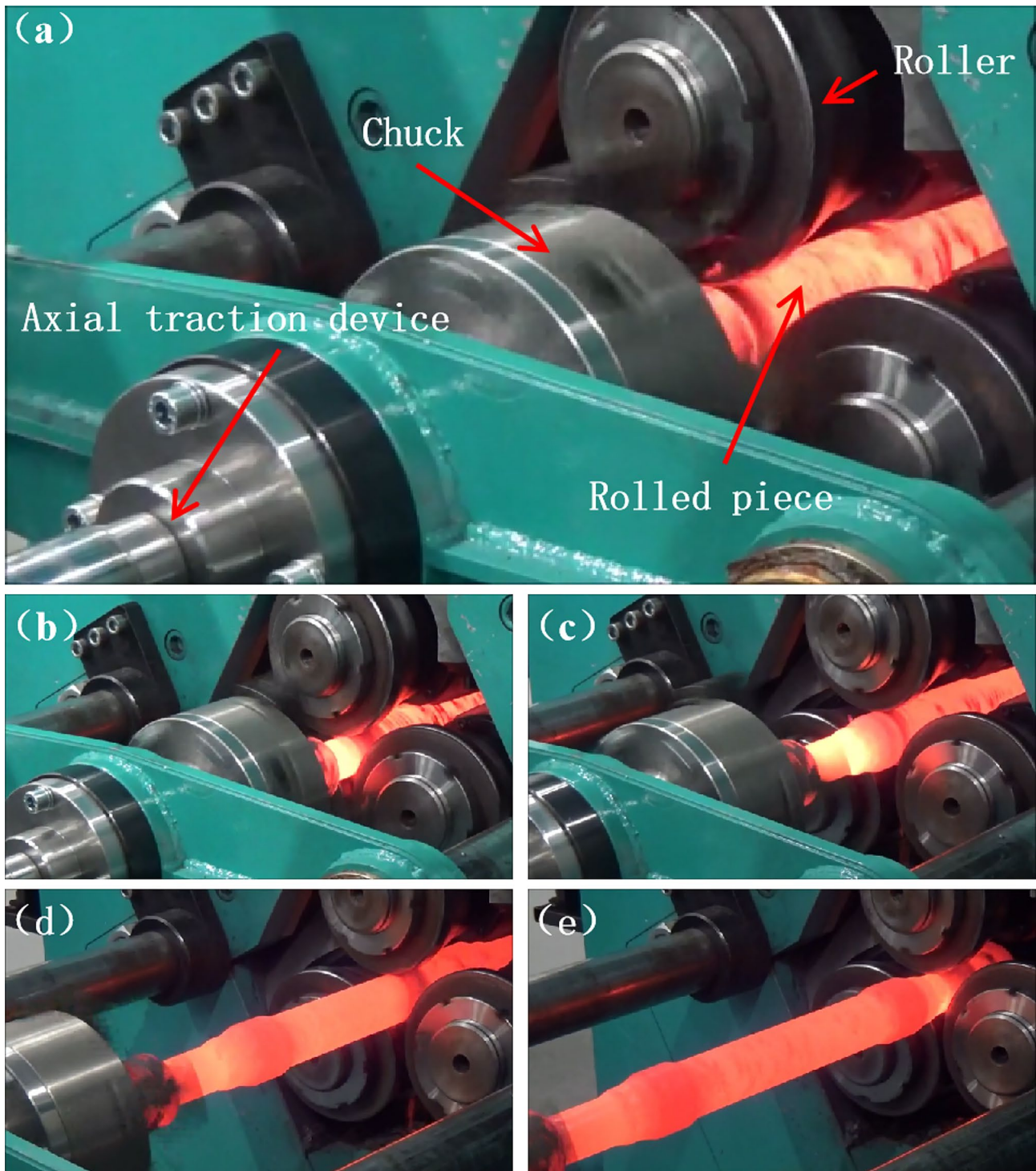


Fig. 5 The forming procedures of the hollow axle in three-roll skew rolling. **a** The rolled piece is set in the TRSR machine after taking from the furnace and begins to deform. **b** Roll piece at the second deformed section, where it has the greater radial compression. **c** Roll

piece at the third deformed section, where it has the smaller radial compression. **d** Roll piece at the end of the fourth deformed section. **e** Roll piece at the sixth deformed section, where it has the same radial compression as the second deformed section

Fig. 6 The rolled piece formed by three-roll skew rolling



3.3 Experimental analysis

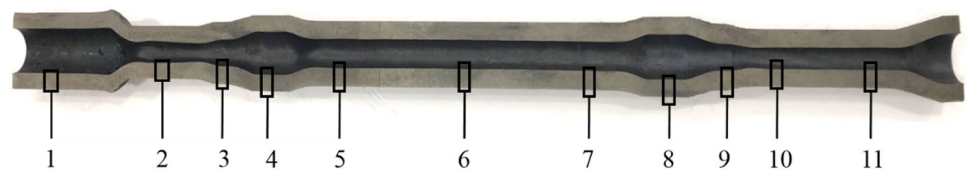
Figure 13 shows the microstructure at the second cross-section, where there is the largest radial compression zone, in the rolled piece no. 1 ($1000\text{ }^{\circ}\text{C}$, $V_z = 20\text{ mm/s}$). Figure 13a–c represent the outer, core, and inner layers, respectively. It can be seen that the grain size is significantly increased from the outer layer to the inner layer. In the meantime, the outer layer has better grain refinement and even distribution, indicating the larger plastic deformation contributes to the grain refinement and distribution. Figure 14 shows the microstructure in the outer layer at cross-sections no. 2, no. 3, and no. 4 in rolled piece no. 1, where the radial compression is correspondingly decreased from no. 2 to no. 4. It can be found with the finest grain at the second cross-section zone and the coarsest grain at the fourth cross-section. This indicates radial compression has a significant influence on the grain size; the larger the radial compression, the better the grain refinement.

The average grain size at all cross-sections of the no. 1 rolled piece is shown in Fig. 15. According to the figure, the

TRSR process can significantly refine the grains, especially in the outer layer of the hollow axle. The radial compression has the most noticeable grain refinement to the outer layer. The greater the radial compression, the better the refinement is. However, radial compression has a limited effect on refinement at the core layer and the inner layer. Compared to the same radial compression, the average grain size is much smaller in the early rolling than in the late rolling part; this phenomenon is more obvious in the core and inner layers.

Figure 16 shows the average grain size at different cross-sections of the no. 2 rolled piece ($T = 1100\text{ }^{\circ}\text{C}$, $V_z = 20\text{ mm/s}$). It can be found that the grain refinement at cross-Sects. 2, 3, and 4 gradually improved with decreasing the radial compression. Interestingly, the same pattern was found at cross-Sects. 8, 9, and 10 with increasing the radial compression. The outer layer is the most consistent one in grain refinement, while the inner and core layers present stochastic patterns. Considering the nature of the rolling process, the outer layer is the direct contact deformation zone. It is inevitable to have more influence on grain refinement on the outer surface

Fig. 7 Locations of the cross-section in the rolled piece for microstructure observation samples



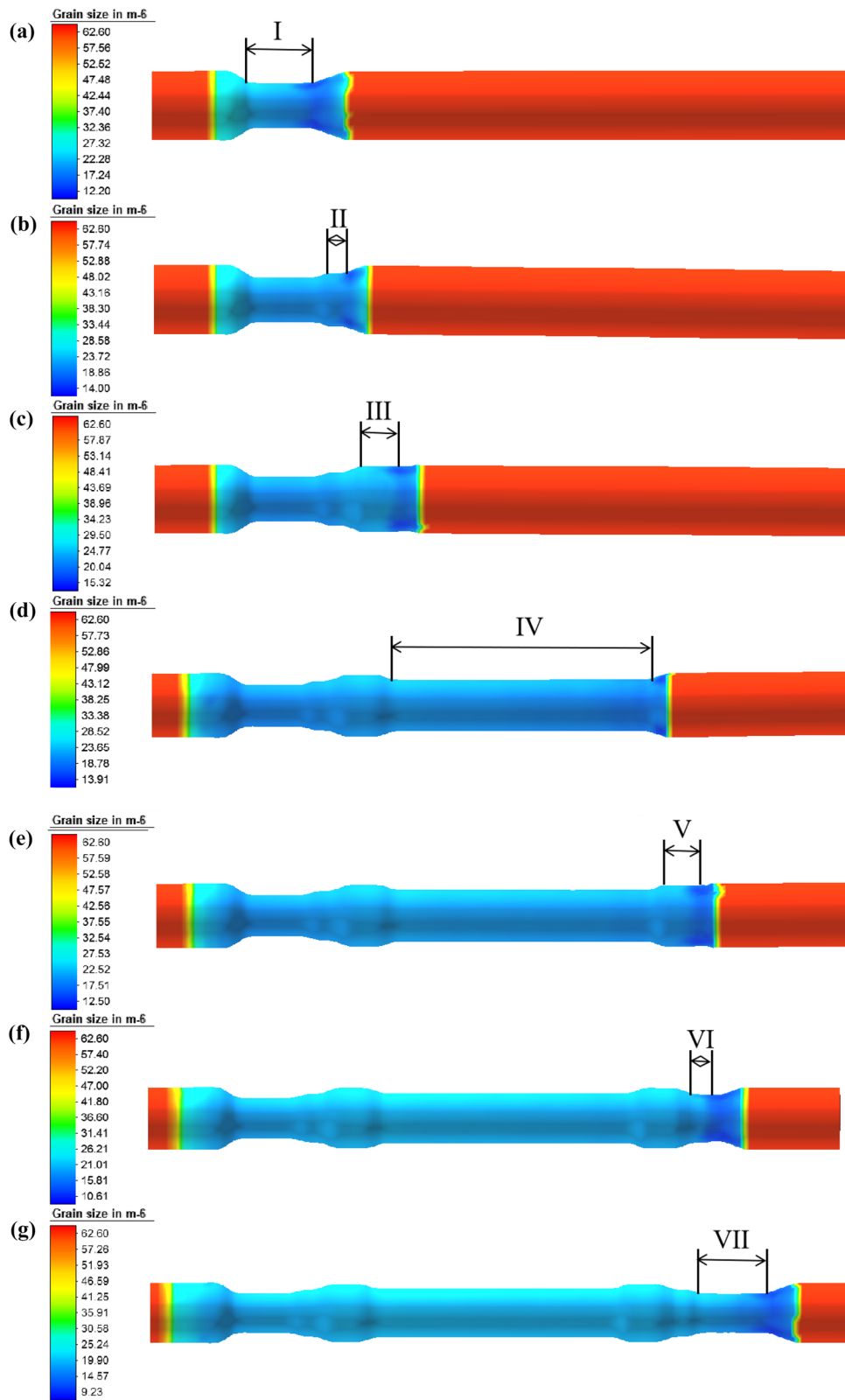


Fig. 8 Microstructure at different stages of the hollow axle by three-roll skew rolling: **a** the first straight shaft section; **b** the second straight shaft section; **c** the third straight shaft section; **d** the fourth

straight shaft section; **e** the fifth straight shaft section; **f** the sixth straight shaft section; **g** the seventh straight shaft section

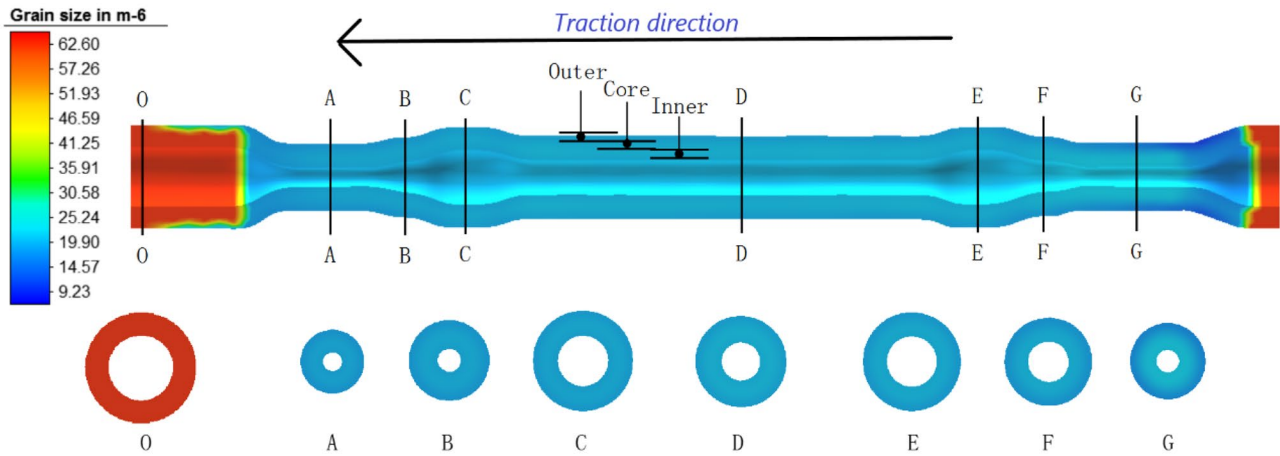


Fig. 9 Microstructure of the 30CrMoA rolled piece with different cross-sections under $T=1100\text{ }^{\circ}\text{C}$, $V_z=20\text{ mm/s}$

than others. Furthermore, grain distribution and grain size in the core and inner layers can be further refined by heat treatment [30].

The no. 1 ($1000\text{ }^{\circ}\text{C}$) and no. 2 ($1100\text{ }^{\circ}\text{C}$) rolled pieces are used to compare the temperature effect on the grain size and microstructure distribution. The initial grain size is affected significantly by the temperature results, going from 22.45 to $62.6\text{ }\mu\text{m}$ as the temperature increases. However, when compared to the relative refinement level, the higher temperature experiences a huge change in regards to the grain size, and the experimental results also agree

with this with the simulation results. Furthermore, when rolling the long shaft parts, the dynamic recrystallization becomes weaker as the length of the shaft increases. This phenomenon is particularly obvious at higher temperatures.

Figure 17 shows the comparison between no. 1 and no. 2 rolled pieces in different layers. The grain size in the outer layer Fig. 17a is refined to $10\text{ }\mu\text{m}$ at $1000\text{ }^{\circ}\text{C}$ and around $15\text{ }\mu\text{m}$ at $1100\text{ }^{\circ}\text{C}$. It can be found that the cross-sections 2–4 present different curve trends at $1000\text{ }^{\circ}\text{C}$ and $1100\text{ }^{\circ}\text{C}$, with the average grain size in no. 2 decreasing

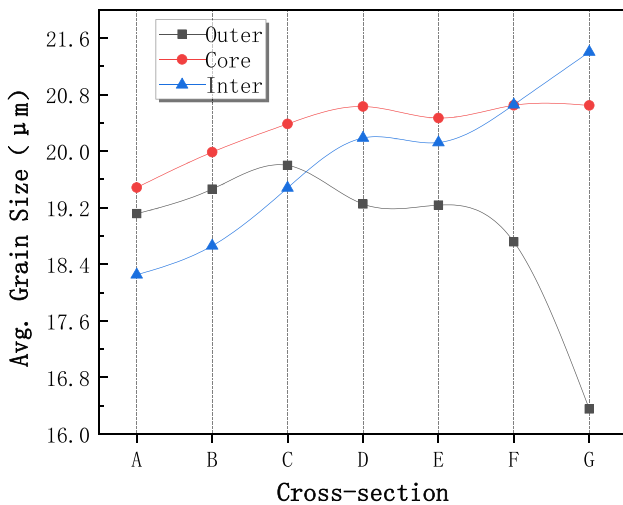


Fig. 10 Grain size distribution at different cross-section under $T=1100\text{ }^{\circ}\text{C}$, $V_z=20\text{ mm/s}$

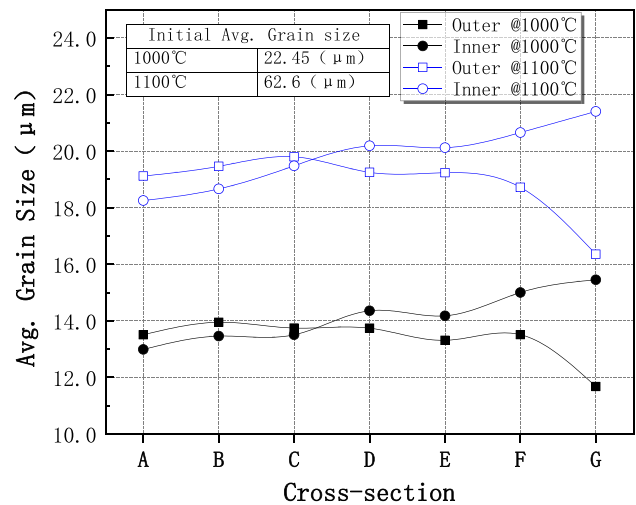


Fig. 11 Average grain size at outer layer and inner layer under two rolling temperatures, $1000\text{ }^{\circ}\text{C}$ and $1100\text{ }^{\circ}\text{C}$

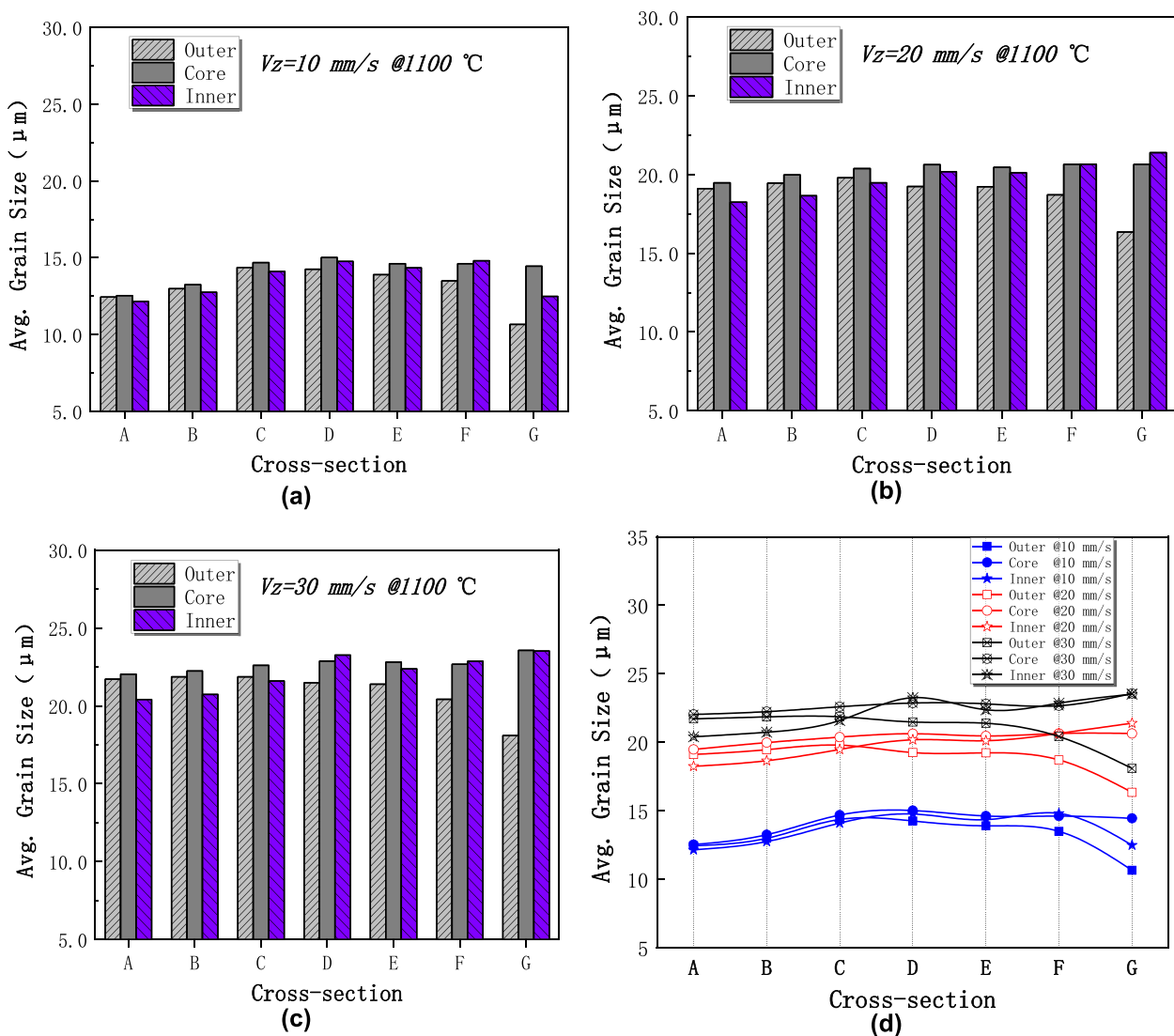


Fig. 12 Average grain size under different axial traction speeds at 1100 °C. **a–c** The grain size distribution at different layer with 10 mm/s, 20 mm/s and 30 mm/s, respectively. **d** Influence of the traction speed on the grain size

instead of increasing at the higher temperature, indicating that the temperature has a significant effect on the outer layer, as the grain refinement by dynamic recrystallization and static grain growth dominate in these sections. Figure 17b presents the grain size distribution in the core layer. The figure shows that in the no. 1 rolled piece, the grain refinement caused by dynamic recrystallization gradually becomes weaker from cross-Sect. 2 to cross-Sect. 8; on the other hand, the grain growth effect is enhanced. In the no. 2 rolled piece, the grain refinement is enhanced from cross-Sect. 2 to cross-Sect. 6, and

the refinement becomes much weaker from cross-Sect. 6 to cross-Sect. 8. Both rolled pieces have a very similar variation trend from cross-Sect. 8 to cross-Sect. 11, and the average grain size of no. 2 is about twice that of no. 1. Results show that the grain refinement in cross-Sects. 8–11 is dominated by recrystallization, and the temperature has a significant influence on the average grain size. Figure 17c shows the grain size at different locations in the inner layer. It can be seen that in the beginning stage of rolling, dynamic recrystallization plays a dominant role in grain refinement. At the lower

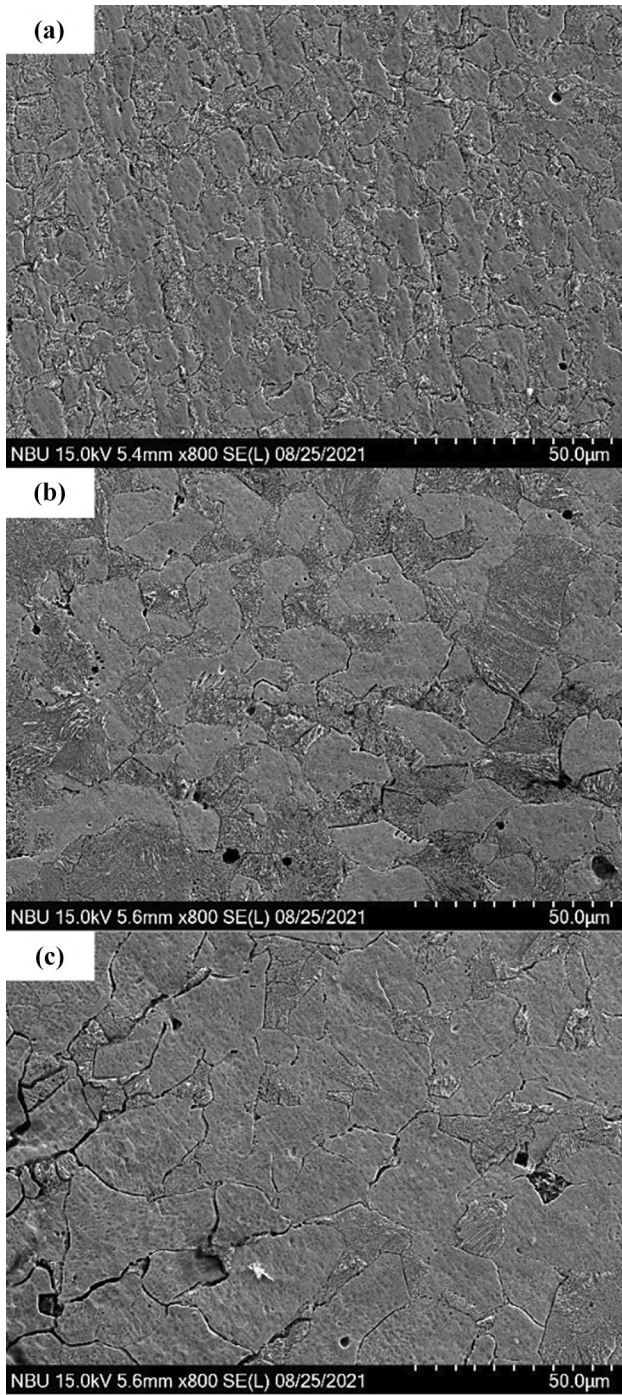


Fig. 13 Grain size of the second cross-section in no. 1 rolled piece (1000 °C, $V_z = 20$ mm/s): **a** outer layer, **b** core layer, and **c** inner layer

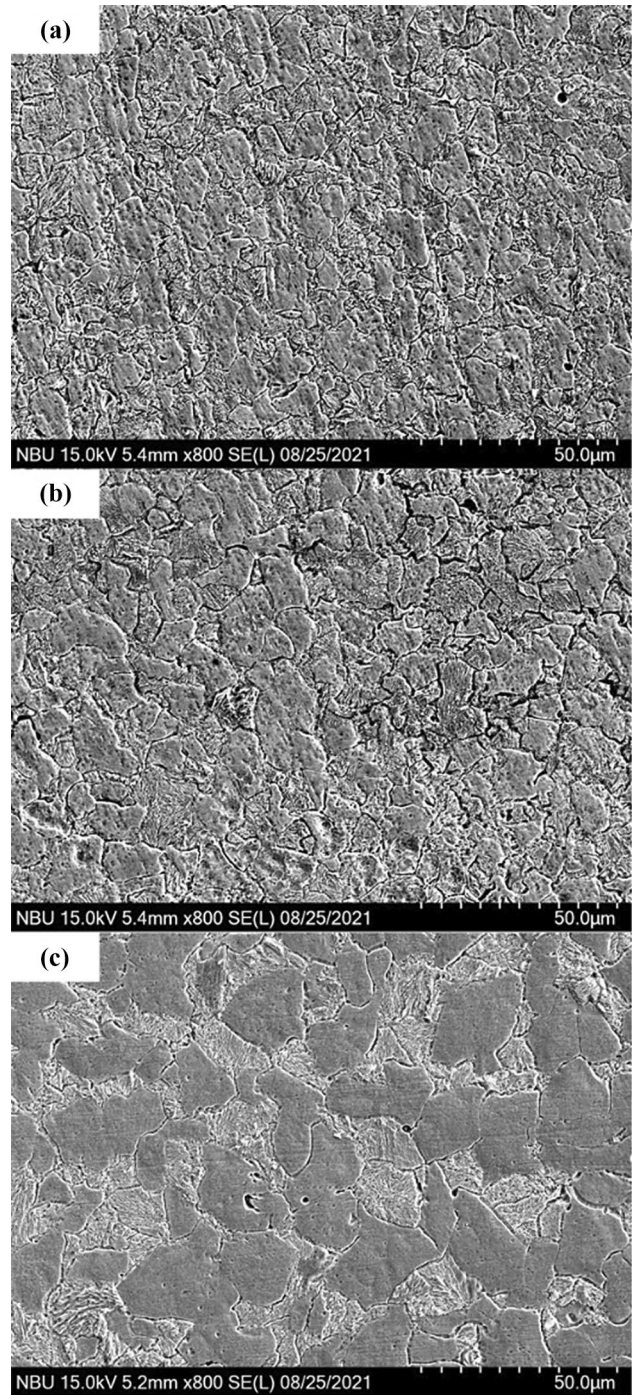


Fig. 14 Grain size of outer layer at different cross-sections in no. 1 rolled piece: **a** no. 2, **b** no. 3, and **c** no. 4

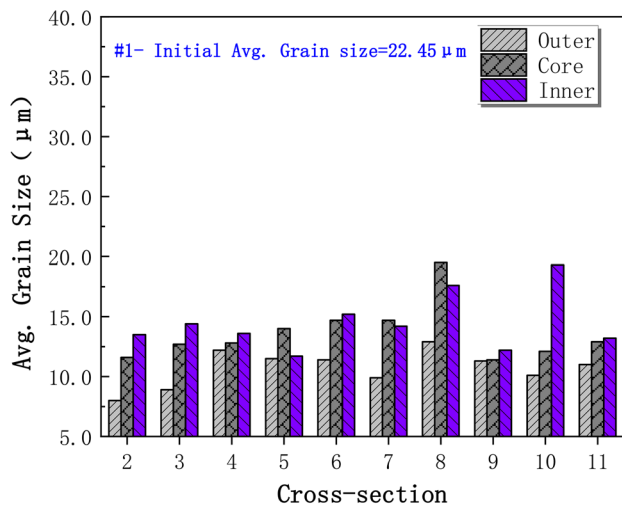


Fig. 15 Average grain size at different cross-sections in no. 1 rolled piece

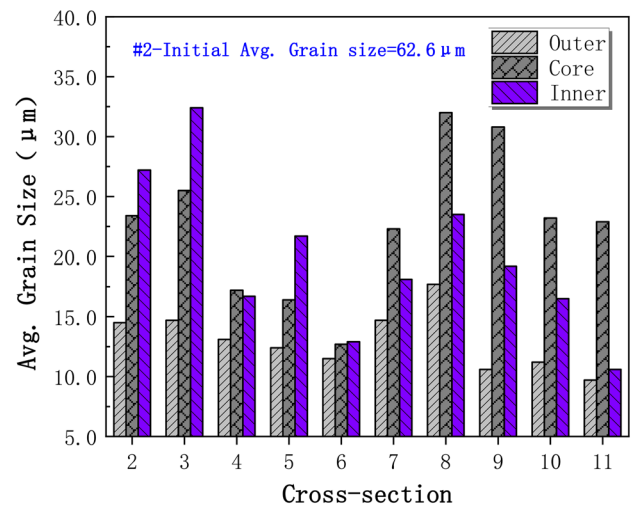


Fig. 16 Average grain size at different cross-sections in no. 2 rolled piece (1100 °C, $V_z=20$ mm/s)

temperature, the growth of recrystallized grains plays a key role in refinement, in particular at the middle and late stages of rolling. At the higher temperature, the growth of recrystallized grains dominates in the middle stage when the radial compression is small. Dynamic recrystallization dominates in the late stage of rolling as the radial compression gradually increases.

In summary, by analyzing the microstructure of the hollow axle in the TRSR process, it can be found that the outer layer has the most refined grain size. Grain size in the first half of the axle along the rolling direction is outer < core < inner and outer < inner < core in the second half. The average grain size in the outer layer is enlarged in the diameter increasing section, vice versa. At lower rolling temperatures, the growth of recrystallized grain dominates in the core layer and inner layer. At higher rolling temperatures, dynamic recrystallization dominates the grain refinement at the core layer in the first half of the axle, and growth of recrystallization dominates the core layer in the second half. Furthermore, as the temperature increased, the final grain size also increased.

3.4 Model validation

As shown in Fig. 18a, the simulation and experimental results are more consistent in the early stage from cross-section A to cross-section D, and there are more fluctuations at cross-sections E and F. It should be noted

that when performing the experiment, the rolled piece is taken from the furnace to the TRSR machine by manual operation. The rolled piece will experience some temperature loss, and the temperature gradient will have a direct impact on the dynamic recrystallization and eventually affect the grain size. Due to the temperature loss during the experiment, the actual grain size is influenced and eventually leads to the difference with the simulation. Figure 18b shows the overall comparison between simulation results and experimental results, which shows the mean and standard deviation of simulation (13.9 ± 0.85 ; 19.6 ± 1.1) and experiment (13.1 ± 2.9 ; 19.3 ± 7.1) at 1000 °C and 1100 °C. The relative error between simulation and experiment is 16.3% (mean absolute error: 2.3 µm) at 1000 °C and 30.7% (mean absolute error: 5.8 µm) at 1100 °C, according to relative error analysis. As discussed in the above section, the microstructure of 30CrMoA is susceptible to higher temperature, in particular at 1100 °C, and the grain size will experience significant changes correspondingly. Due to this reason, the temperature loss at higher temperatures plays a huge impact on the final grain size and the larger differences occurred between simulation and experiments. In Fig. 18c, the trends of microstructure evolution in simulation and experiment are consistent with the polynomial fit, and the fitting equation can be further used to precisely predict the experiment with the appropriate offset. In summary, the established constitutive model provides valuable information and can be used to predict the microstructure evolution of TRSR.

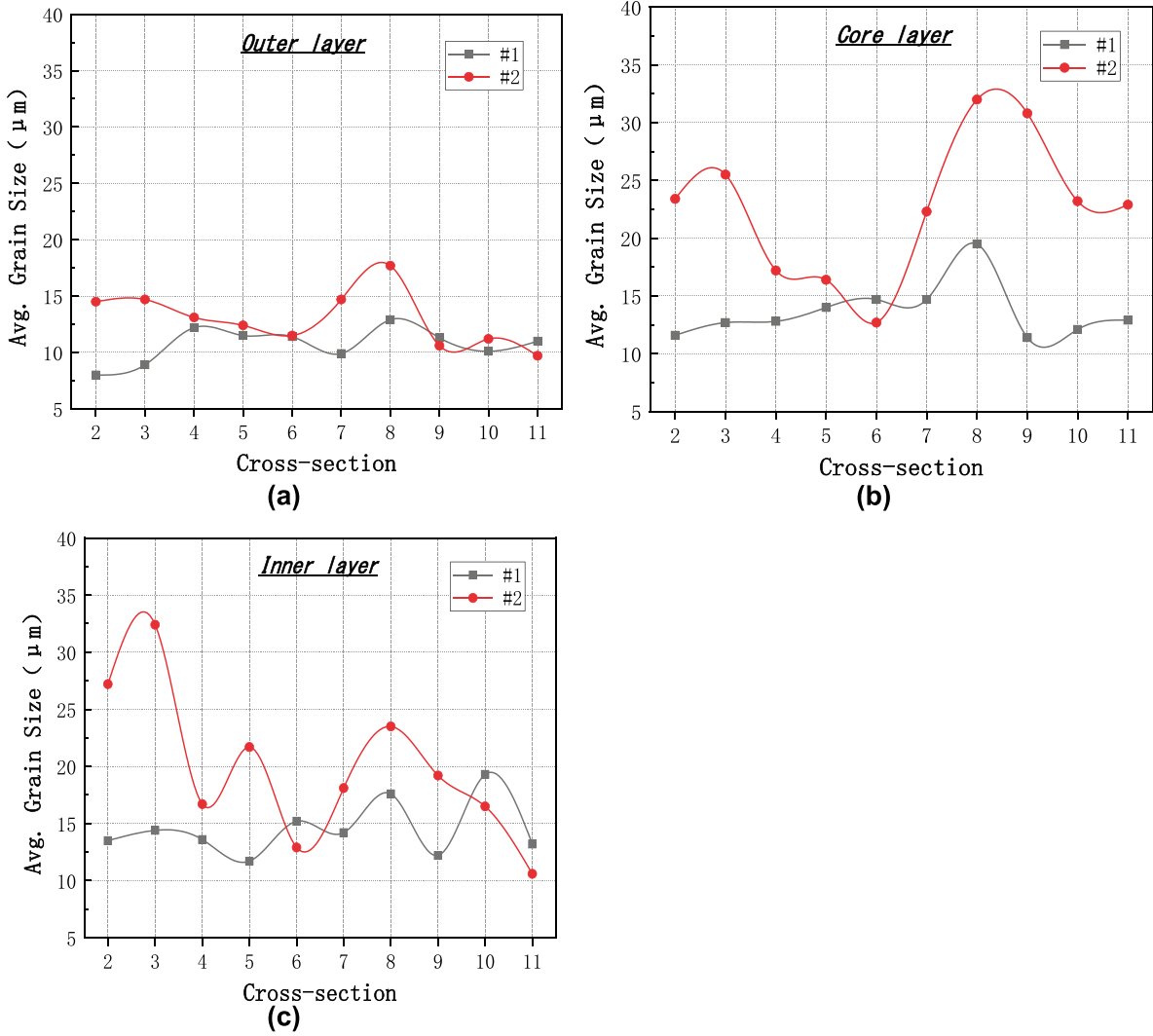
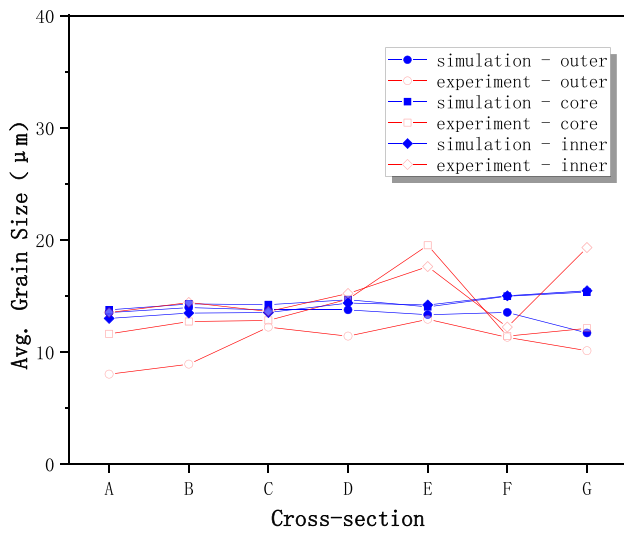
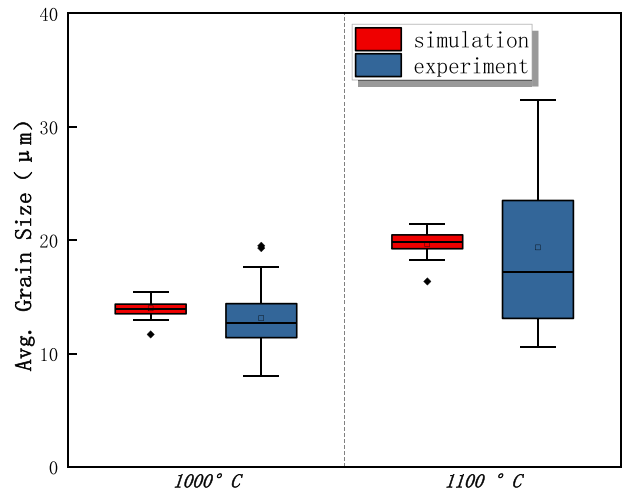


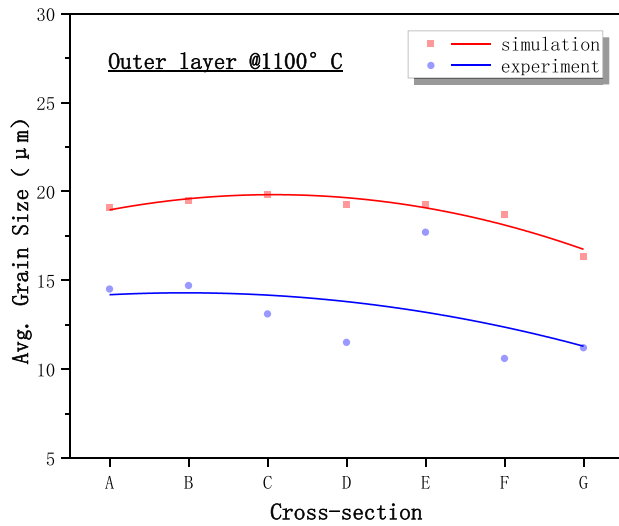
Fig. 17 Comparison of average grain size at different layers between no. 1 rolled piece and no. 2 rolled piece. **a** Grain size comparison in the outer layer. **b** Grain size comparison in the core layer. **c** Grain size comparison in the inner layer



(a)



(b)



(c)

Fig. 18 **a** Comparison of the average grain size between experiment and simulation at 1000 °C. **b** Comparison of overall average grain size between experiment and simulation by three-roll skew rolling. **c**

The polynomial regression of simulation and experimental results in outer layer at 1100 °C

4 Conclusion

1. Three-roll skew rolling can refine the microstructure. At lower temperatures, the initial grain size is relatively small and the effect on refinement is not obvious. With the temperature rising, the initial grain size gets larger and the effect on refinement is significant.
2. The axial traction speed has a moderate influence on the microstructure in three-roll skew rolling. The greater the axial traction speed, the larger the average grain size. The increasing rate of grain size decreases with the increase in axial traction speed. At 1100 °C, the aver-

- age grain size of 10 mm/s is the smallest, while the grain size is most evenly distributed at 20 mm/s.
3. The radial compression has a significant impact on average grain size. The greater the radial compression, the finer the grain size, and the more evenly distributed is. The outer layer has the finest average grain size, while the grain size in the core and inner layers depends on the location in the hollow axle. In the first half of the axle, where the diameter of the rolled piece is gradually increasing, the core layer has a smaller grain size than the inner layer. In the second half, where the diameter is gradually decreasing, the core layer has a larger grain

size than the inner layer. All three layers can be refined by the three-roll skew rolling process. Furthermore, the finest refinement in the outer layer is beneficial to improving the surface properties of rolled-piece.

- By comparing the results between the simulation and experiment, the established constitutive model can reflect the microstructure evolution during the three-roll skew rolling process and provide valuable information for future numerical simulation.

Author contribution Chang Shu: conceptualization, methodology, investigation, formal analysis, and writing—original draft. Song Zhang: material preparation, data collection, and writing—review and editing. Prveen Bidare: writing—review and editing. Khamis Essa: supervision, writing—review and editing. Adel Abdel-Wahab: writing—review and editing. Xuedao Shu: writing—review and editing; supervision; funding acquisition; project administration. Zbigniew Pater: material preparation. Jaroslaw Bartnicki: material preparation. All authors read and approved the final manuscript.

Funding The research was funded by the National Natural Science Foundation of China (grant number: 51975301), Key Fund Projects of Zhejiang Province (grant number: LZ22E050002).

Declarations

Competing interests The authors declare no competing interests.

Open Access This article is licensed under a Creative Commons Attribution 4.0 International License, which permits use, sharing, adaptation, distribution and reproduction in any medium or format, as long as you give appropriate credit to the original author(s) and the source, provide a link to the Creative Commons licence, and indicate if changes were made. The images or other third party material in this article are included in the article's Creative Commons licence, unless indicated otherwise in a credit line to the material. If material is not included in the article's Creative Commons licence and your intended use is not permitted by statutory regulation or exceeds the permitted use, you will need to obtain permission directly from the copyright holder. To view a copy of this licence, visit <http://creativecommons.org/licenses/by/4.0/>.

References

- Gao Y, Su W, Wang K (2019) Does high-speed rail boost tourism growth? New evidence from China Tourism Management 72:220–231. <https://doi.org/10.1016/j.tourman.2018.12.003>
- Yu M, Fan W (2018) Accessibility impact of future high speed rail corridor on the piedmont Atlantic megaregion. J Transp Geogr 73:1–12. <https://doi.org/10.1016/j.jtrangeo.2018.09.014>
- Li H-X, Wang K, Luo R, Zhu Z-Z, Deng S, Luo R et al (2020) Influence of radial forging process on strain inhomogeneity of hollow gear shaft using finite element method and orthogonal design. J Cent South Univ 27(6):1666–1677. <https://doi.org/10.1007/s11771-020-4398-7>
- Zhang S, Shu X, Xia Y, Wang J (2021) Formation mechanism and control of the spiral marks of three-roll skew-rolled hollow axles. Metalurgija 60(1–2):51–54
- Bartnicki J, Pater Z (2005) Numerical simulation of three-rolls cross-wedge rolling of hollowed shaft. J Mater Process Technol 164–165:1154–1159. <https://doi.org/10.1016/j.jmatprotec.2005.02.120>
- Bartnicki J, Pater Z (2004) The aspects of stability in cross-wedge rolling processes of hollowed shafts. J Mater Process Technol 155–156:1867–1873. <https://doi.org/10.1016/j.jmatprotec.2004.04.278>
- Zhang S, Shu X, Xu C, Wang J, Li Z (2019) Research on wall thickness uniformity of hollow axles by three-roll skew rolling. ASME Int Mech Eng Congress Expos V02AT02A029. <https://doi.org/10.1115/imece2019-10486>
- Pang H, Lowrie J, Ngaile G (2017) Development of a non-isothermal forging process for hollow axle shafts. Procedia Eng 207:454–459. <https://doi.org/10.1016/j.promfg.2018.07.087>
- Winiarski G, Gontarz A, Samolyk G (2020) Theoretical and experimental analysis of a new process for forming flanges on hollow parts. Materials (Basel) 13(18). <https://doi.org/10.3390/ma13184088>
- Wang J, Shu X, Zhang S, Li S, Pater Z, Xia Y et al (2021) Research on microstructure evolution of the three-roll skew rolling hollow axle. Int J Adv Manuf Technol 118(3–4):837–847. <https://doi.org/10.1007/s00170-021-07991-7>
- Shu X-D, Zhang S, Ehmann KF, Li Z-X, Wei Y-L (2020) Forming and uniformity of shaft parts without a stub bar by axial closed-open-type cross-wedge rolling. J Iron Steel Res Int 27(9):1054–1063. <https://doi.org/10.1007/s42243-020-00459-0>
- Zhang N, Wang B-Y, Lin J-G (2012) Effect of cross wedge rolling on the microstructure of GH4169 alloy. Int J Miner Metall Mater 19(9):836–842. <https://doi.org/10.1007/s12613-012-0636-9>
- Zhang S, Shu X, Xu C, Wang J, Xia Y (2020) Simulation and experiment of reduction of equal-diameter hollow shafts with three-roll skew rolling. Procedia Manuf 50:183–186. <https://doi.org/10.1016/j.promfg.2020.08.034>
- Cao X, Wang B, Zhou J, Shen J, Lin L (2021) Exploratory experiment and numerical simulation investigation on a novel flexible skew rolling of hollow shafts. Int J Adv Manuf Technol 116(11):3391–3403. <https://doi.org/10.1007/s00170-021-07360-4>
- Xu C, Shu X (2018) Influence of process parameters on the forming mechanics parameters of the three-roll skew rolling forming of the railway hollow shaft with 1: 5. Metalurgija 57(3):153–156
- Stefanik A, Morel A, Mroz S, Szota P (2015) Theoretical and experimental analysis of aluminium bars rolling process in three-high skew rolling mill. Arch Metall Mater 60(2A):809–813. <https://doi.org/10.1515/amm-2015-0211>
- Gryc A, Bajor T, Dyja H (2016) The analysis of influence the parameters of rolling process in three high skew rolling mill of AZ31 magnesium alloy bars on temperature distribution. Metalurgija 55(4):772–774
- Markov O, Gerasimenko O, Khvashchynskiy A, Zhytnikov R, Puzyr R (2019) Modeling the technological process of pipe forging without a mandrel. East-Eur J Enterp Technol 3(1–99):42–48. <https://doi.org/10.15587/1729-4061.2019.167077>
- Pater Z (2017) FEM analysis of loads and torque in a skew rolling process for producing axisymmetric parts. Arch Metall Mater. <https://doi.org/10.1515/amm-2017-0011>
- Peter Z, Bulzak T, Tomczak J (2016) Numerical analysis of a skew rolling process for producing a stepped hollow shaft made of titanium alloy Ti6Al4V. Arch Metall Mater. <https://doi.org/10.1515/amm-2016-0115>
- Pater Z, Tomczak J, Bulzak T (2015) Numerical analysis of the skew rolling process for main shafts. Metalurgija 54(4):627–630
- Pater Z, Tomczak J, Bulzak T (2020) Problems of forming stepped axles and shafts in a 3-roller skew rolling mill. J Mater Res Technol 9(5):10434–10446. <https://doi.org/10.1016/j.jmrt.2020.07.062>

23. Bartnicki J, Xia Y, Shu X (2021) The chosen aspects of skew rolling of hollow stepped shafts. *Materials* 14(4):764. <https://doi.org/10.3390/ma14040764>
24. Zhang S, Shu X, Wang J, Xu C (2020) Deformation behavior of hollow axles with constant hole diameter by three-roll skew rolling. ASME 2020 International Mechanical Engineering Congress and Exposition. V02AT02A025: American Society of Mechanical Engineers. <https://doi.org/10.1115/IMECE2020-23225>
25. Zhang S, Shu X, Wang J, Ye C (2021) Formation and control of defects on the surface of hollow axles by three-roller skew rolling. ASME 2021 International Mechanical Engineering Congress and Exposition. V02AT02A044: American Society of Mechanical Engineers. <https://doi.org/10.1115/IMECE2021-68789>
26. Zheng Y, Wang F, Li C, Li Y, Cheng J, Cao R (2018) Effect of microstructure and precipitates on mechanical properties of Cr–Mo–V alloy steel with different austenitizing temperatures. *ISIJ Int* 58(6):1126–1135. <https://doi.org/10.2355/isijinternational.ISIJINT-2017-531>
27. Beretta S, Carboni M, Cantini S, Ghidini A (2004) Application of fatigue crack growth algorithms to railway axles and comparison of two steel grades. *Proc Inst Mech Eng Part F J Rail Rapid Transit* 218(4):317–326. <https://doi.org/10.1243/0954409043125888>
28. Zhang S, Shu X, Wang J, Xia Y (2020) Constitutive Model of 30CrMoA steel with strain correction. *Metals* 10(9):1214. <https://doi.org/10.3390/met10091214>
29. Shu X, Zhang S, Wang J, Shi J, Xia Y (2020) Flow stress behavior of 30CrMoA steel under high temperature compression. *Metallurgija* 59(3):313–316
30. Guo K, Meng K, Miao D, Wang Q, Zhang C, Wang T (2019) Effect of annealing on microstructure and tensile properties of skew hot rolled Ti–6Al–3Nb–2Zr–1Mo alloy tube. *Mater Sci Eng A* 766:138346. <https://doi.org/10.3390/met10091214>

Publisher's note Springer Nature remains neutral with regard to jurisdictional claims in published maps and institutional affiliations.